

may contribute a similar amount to the observed splittings. The radial functions of Rajnak¹⁰ indicate that overlap contributions for $5d$ electrons will certainly be more important than for $4f$ electrons and may be comparable to the values encountered in the $3d$ transition-metal complexes; also the off-diagonal elements will be modified. Under these conditions, all the short-range contributions to the potential from the nearest-neighbor fluorine ions ought to be considered separately and a cluster calculation used to project out the contributions

from every phonon. This will modify the contributions to Y_1 from phonons away from the Γ point, but the effect on Y_3 will be more serious. Nevertheless, the present calculations give a clear indication of the reasonable degree of accuracy to be expected from a crystal-field calculation. Our approximations have yielded values for the amplitudes of the multipole contributions within a factor of 3 of the experimental values, though more serious discrepancies of the same magnitude remain in the frequency dependence of some of these terms.

*Research supported by the Joint Services Electronics Program, through the Air Force Office of Scientific Research (AFSC), under Contract No. F 44620-71-C-0067.

†Work supported in part by Volkswagen Foundation.

¹M. Wagner, *Z. Physik* **214**, 78 (1968).

²D. L. Wood and W. Kaiser, *Phys. Rev.* **126**, 2079 (1962).

³H. V. Laver, D. H. Kuhner, and W. E. Bron, *Bull. Am. Phys. Soc.* **16**, 427 (1971).

⁴J. P. Hurrell and V. J. Minkiewicz, *Solid State Commun.* **8**, 463 (1970).

⁵B. R. Judd, *Phys. Rev.* **127**, 750 (1962).

⁶J. D. Axe, *Phys. Rev.* **136**, 43 (1964).

⁷R. A. Cowley, W. Cochran, B. N. Brockhouse, and A. D. B. Woods, *Phys. Rev.* **131**, 1020 (1963).

⁸T. Timusk and M. V. Klein, *Phys. Rev.* **141**, 664 (1966).

⁹R. A. Cowley, *Acta. Cryst.* **15**, 687 (1962).

¹⁰K. Rajnak, *J. Chem. Phys.* **37**, 2440 (1962).

¹¹A. J. Freeman and R. E. Watson, *Phys. Rev.* **127**, 2058 (1962).

¹²B. R. Judd, *Proc. Roy. Soc. (London)* **228A**, 120 (1955).

¹³C. W. Nielson and G. F. Koster, *Spectroscopic Coefficients for the p^n , d^n and f^n Configurations* (MIT Press, Cambridge, Mass., 1963).

¹⁴A. J. Freeman and R. E. Watson, *Phys. Rev.* **139**, 1606 (1965).

¹⁵A. J. Freeman and R. E. Watson, *Phys. Rev.* **156**, 251 (1967).

Mössbauer Study of Gold-Iron Alloys*

B. Window

Materials Physics Division (8), Atomic Energy Research Establishment, Harwell, United Kingdom and Physics Department, Carnegie-Mellon University, Pittsburgh, Pennsylvania 15213

(Received 29 November 1971)

Mössbauer results obtained at 300 and 4.2 K for Fe^{57} in alloys of 2–40 at. % iron in gold have been fitted with consistent values for the hyperfine interactions. The 300-K data are adequately fitted using a reducing-point-charge model based on a Thomas-Fermi-like model for the iron screening in gold, and the derived parameters are used in fitting the 4.2-K data. The sign of the electric field gradient is deduced to be negative, and information concerning the magnetic moment alignment with different numbers of neighbors is derived. The spins point along $\langle 111 \rangle$ crystallographic directions when the atom has two or more iron neighbors, and along directions normal to the iron-iron axis when it has one neighbor. With increased size of groups of atoms the spins point along the $\langle 111 \rangle$ axis that minimizes the number of Fe-Fe axes normal to it, until at about 16 at. % iron long-range ferromagnetism occurs due to the occurrence of linear chains. The results for higher-concentration alloys are consistent with those expected for a ferromagnetic random alloy.

I. INTRODUCTION

Gold-iron alloys have been studied using the Mössbauer technique with Fe^{57} ,^{1–11} Sn^{119} ,^{12,13} and Au^{197} ¹⁴ nuclei, and considerable information concerning the magnetic ordering has been obtained. However, in the case of Fe^{57} where complicated spectra are obtained above and below the ordering temperatures, a model which accounts for the spec-

tra at both high and low temperatures and over a range of iron concentration has not been proposed. The Fe^{57} resonance shows distributions of isomer shifts, quadrupole splittings, and magnetic splittings, and while the analysis of the spectra is difficult because of these distributions, a careful interpretation can yield valuable information about the magnetic moment alignment with respect to the atomic neighbors. Also there has occurred in the

literature a number of incorrect explanations concerning the apparent lack of a quadrupole splitting when magnetically ordered, and the aim is to correct these misinterpretations.

The earlier work concentrated on the broad features of the spectra for the dilute alloys containing less than 15 at. % iron. Violet and Borg⁵ showed that below the magnetic-ordering temperature given by $T_0 = 11.6c^{1/2}$, where c is the iron concentration in atomic percent, sharp six-line magnetic spectra were observed. The spectra above the ordering temperature, which apparently consisted of a single line and a doublet, were interpreted in terms of quadrupole interactions due to near-neighbor iron atoms,⁶ and Ridout⁸ showed that the asymmetry of the doublet, which was accounted for by Borg⁷ by invoking a Goldanski-Karayagin effect,¹⁵ was in fact a consequence of there being iron atoms with a distribution of numbers of iron neighbors. Ridout⁸ also showed that the low-temperature spectra contained a significant amount of fine detail, which previous workers had not observed, and managed to fit the spectra assuming a random distribution of iron atoms, and assigning electric field gradients, isomer shifts, and magnetic fields to iron atoms depending on the number of iron near neighbors. However, there was little correspondence between his fitted parameters describing the isomer shifts above and below the ordering temperature, and the parameters describing the low-temperature fit were almost certainly incorrect.

A mechanism to produce these large electric field gradients at iron nuclei in noble-metal-based alloys was proposed by Window¹¹ from a study of Fe⁵⁷ in AuX alloys, where X is a $3d$ impurity. Within the framework of a Thomas-Fermi-like model^{16,17} for the distribution of the iron screening charge around the nucleus, the radial distribution of charge $\rho(r)$ around an impurity of charge Z_0 is given by

$$\rho(r) = - (1/16\pi^2) Z_0 \lambda^2 e^{-\lambda r} / r, \quad (1)$$

$$\lambda^2 = 4\pi n(E_F), \quad (2)$$

and $n(E_F)$ is the density of states at the Fermi level ($\lambda = 1.8 \text{ \AA}^{-1}$ for gold). An iron atom in gold which has twelve gold first neighbors will have a screening charge distribution of cubic symmetry (hence no electric field gradient at the nucleus) and the majority of the necessary screening electrons (Z_0) will be localized within the atomic cell. On the virtual-bound-state theory¹⁸⁻²⁰ for these alloys of transition metals in noble metals, this excess charge will be accommodated below the Fermi level in a d resonance in the host conduction band, the distribution of excess states in energy being Lorentzian in form and accommodating in all ten

states. This resonance will generally produce an increase in the density of states at the Fermi level localized on the X atom, and it is this increase which causes the screening charge of an iron impurity to distort when an X atom is placed in a near-neighbor position. This mechanism explains the correspondence observed between the residual resistivity per percent X of gold- X alloys,²⁰ and the electric field gradient (efg) and isomer-shift changes induced at an iron nucleus by an X neighbor in gold.¹¹ This model can be discussed in terms of an effective point charge localized on the neighboring site but describing the distortion of the screening charge on the central atom.²¹ A further consequence of this model is that one expects the effective point charge to decrease with increasing numbers of X neighbors.¹¹

The objects of the investigation reported here were to fit the 300-K spectra of gold-iron alloys over a wide concentration range with a minimum set of parameters, and to use these parameters to fit the 4.2-K data, giving information concerning the spin directions in these alloys. The fitting also shows that the Debye-Waller factor is reduced by a near-neighbor iron atom and is probably anisotropic. The difference in the areas of the quadrupole peaks suggests that the sign of the electric field gradient is negative. Using the high-temperature parameters, the 4.2-K data give, besides the magnitudes of the hyperfine fields for iron atoms with $n = 0, 1,$ and 2 or more neighbors, the orientations of the spins with respect to the near-neighbor iron atoms. Some information concerning the applicability of the random antiferromagnet model proposed for these alloys^{22,23} was derived. The spectra for the alloys show how the type of magnetic order changes with changing iron concentration, the spins in concentrated alloys tending to point along $\langle 111 \rangle$ crystallographic directions.

II. EXPERIMENTAL DETAILS

Conventional Mössbauer spectrometers of high linearity and low drift were used to obtain the spectra. Top-loading helium and nitrogen Dewars²⁴ were used to obtain the spectra at low temperatures, and one sample was heated to 400 K in a small Mössbauer furnace.

The sources used, 100 mCi of Co⁵⁷ diffused into 6- μm palladium foils,²⁵ were maintained at 298 K during the experiments, and curve fitting the spectra obtained using a thin iron absorber (6 μm of natural iron) yielded a joint linewidth of 0.21 mm/sec for the inner two lines. All calibrations were done using either this iron foil or one enriched with Fe⁵⁷, and the velocity scales and isomer shifts are all with respect to this standard.²⁶

The alloys were prepared by argon arc melting the required amounts of iron and gold, the iron

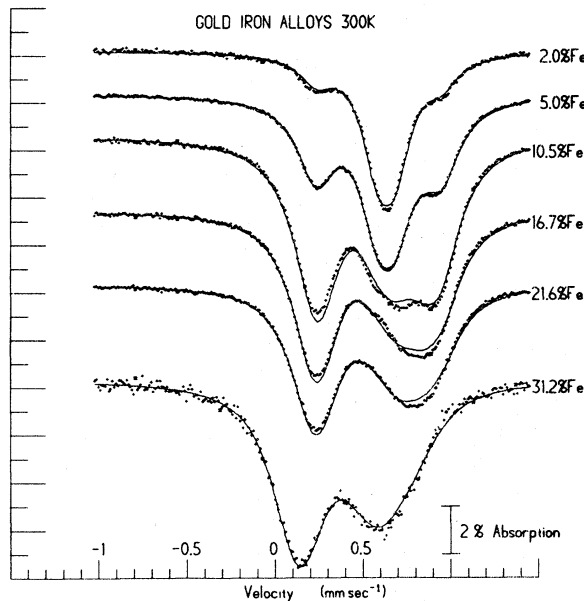


FIG. 1. Mössbauer spectra obtained at 300 K for AuFe (2–21 at. %) alloys, and at 400 K for a AuFe 30-at. % sample are shown. The full lines are fitted curves explained in the text. The zero of velocity is the center of the α -iron spectrum.

being enriched so that there was approximately a constant amount of Fe^{57} (~ 4 at. %) in each sample. This restricting of the Fe^{57} concentration is to minimize line-broadening effects in the iron-rich samples.²⁷ After melting, the alloys were cold rolled to 6–8- μm foils and used in this condition. Mössbauer work on unstable copper-iron alloys²⁸ has shown that this treatment results in more random alloys than are obtained by conventional quenching, since the heavy cold rolling breaks up preprecipitation clusters. Quenched alloys gave substantially the same spectra and no evidence of a second phase was observed in the Mössbauer spectra of the as-rolled samples.

III. RESULTS AND DISCUSSION

A. Electrostatic Interactions

1. Concentration Dependence

The Mössbauer spectra of alloys containing < 35 at. % iron at temperatures above their magnetic-ordering temperatures are shown in Fig. 1. The spectra of the lower-percentage alloys show the features reported by other authors,^{6–8,11} in particular a single line produced by iron nuclei without iron neighbors, and a doublet produced by the electric field gradient at the nuclei of iron atoms with iron neighbors. The shape of the spectra at higher iron concentrations is best described as a doublet with one broad and one narrow line.

Initial attempts to fit these spectra were based

on the following model, which is similar to that employed by Preston *et al.*²¹ to fit spectra of VFe alloys. A nucleus of Fe^{57} with n iron nearest neighbors in a particular arrangement β , labeled by $C(n, \beta)$, was assigned an isomer shift of $(\Delta + n\delta)$ mm/sec, and an electric field gradient giving a splitting of $Q_1 f(n, \beta)$ mm/sec in the Mössbauer spectrum, where Δ is the isomer shift of the isolated iron atom, δ is the isomer-shift change per iron neighbor, and Q_1 is the splitting (in mm/sec) due to the efg in a configuration with one iron and eleven gold near neighbors. The factor $f(n, \beta)$ was calculated for the configuration $C(n, \beta)$ by finding the components of the efg tensor for a point charge on each iron atom in the configuration, diagonalizing to determine V_{zz} , the largest in magnitude principal value of the efg tensor, and η , the asymmetry parameter,²⁹

$$\eta = |(V_{xx} - V_{yy})/V_{zz}|, \quad (3)$$

and calculating the quadrupole splitting

$$f(n, \beta) = AV_{zz}(1 + \frac{1}{3}\eta^2)^{1/2}, \quad (4)$$

where A is a constant fixed by making

$$f(1, \beta) = 1. \quad (5)$$

All possible configurations $C(n, \beta)$ for $n = 0–12$ were considered in the fitting; the intensities of the various components being calculated assuming the alloys were random solid solutions. The linewidth was fixed at 0.21 mm/sec full width at half-maximum.

With these constraints satisfactory fits were not obtained. Firstly, for the more dilute samples the peak due to the isolated iron nuclei was broadened, as has been previously reported,^{6–8} and secondly, the values of Q_1 derived in the fitting showed a marked decrease with increasing iron concentration. Mössbauer studies of Fe-Fe pairs in copper²⁸ show an efg of 0.56 mm/sec compared with 0.7 mm/sec^{6,8} in gold, and so one does not expect a large falloff in Q_1 on the basis of a change in lattice parameter alone.

The first effect is clearly due to efg's produced by neighbors further removed than the nearest shell, and they should be included in the calculation. The broadening of the central peak was simulated by replacing the single line by a pair of Lorentzian lines of equal intensities and widths^{6–8} separated by 0.1 mm/sec; a value which was determined by allowing it to vary when fitting the data for the 2- and 5-at. %-iron samples, and which was subsequently fixed in fitting all the spectra. This procedure is adequate for the effects of the further neighbors on iron atoms with no iron near neighbors, but would be unsatisfactory in treating these interactions at nuclei which already had at least one iron near neighbor. The effect of this

small additional efg [giving a quadrupole splitting by itself of $Q^1 = 0.1$ mm/sec ($Q^1 \sim \frac{1}{7} Q_1$)] can be evaluated for any angle subtended at the origin by the two point charges either numerically as described earlier, or by treating Q^1 as a perturbation on Q . The limiting cases are clearly when the angle between their lattice vectors is zero, giving a resultant $Q_1 + Q^1$, and $\frac{1}{2}\pi$ giving a resultant $Q_1 - \frac{1}{2}Q^1$ (for $Q^1 \ll Q_1$). The observation of significant broadening of the isolated iron nuclear resonance for concentrations as low as 2 at. % iron shows that at least (6+24) further neighbors contribute significant values of Q^1 . The effect of this large number of sites can be approximated by moving Q^1 uniformly over a sphere while keeping Q_1 fixed. A distribution of quadrupole splittings is obtained and the probability of a quadrupole splitting Q between the limits $Q_1 - \frac{1}{2}Q^1$ to $Q_1 + Q^1$ (see Appendix) is given by

$$p(Q)dQ = 3^{-1/2} dQ/Q^1 [1 + 2(Q - Q_1)/Q^1]^{1/2},$$

$$Q^1 \ll Q_1. \quad (6)$$

The principal effect of this distribution, similar to Fig. 7, is to broaden each line of the quadrupole doublet due to Q_1 in an asymmetric fashion, and the sign of the asymmetry will depend on the relative signs of Q_1 and Q^1 . The distribution of splittings of the doublet will result in a smaller broadening of each of these lines than was observed for the line due to the isolated iron nuclei (0.1 mm/sec) and we have chosen to include this broadening in an approximate fashion by allowing the linewidth to vary to minimize the sum of squares at some value greater than 0.21 mm/sec full width half-maximum.

The second problem concerns the reducing value of the point charge per neighbor. The model so far assumes that the point charge localized in an Fe-Fe direction is independent of the number (n) of iron near neighbors. However, this is a poor assumption, and if it is assumed that the screening charge localized along an Fe-near-neighbor axis is equal to a constant plus a term proportional to the density of states on the neighbor,¹¹ it is easy to show that the difference in charge Q_n between that localized on each of the n Fe-Fe axes and that localized on each of the (12- n) Fe-Au axes is given by¹¹

$$Q_n = 12 Q_0 f(n, \beta) / (12 + \alpha n) \quad \text{for } n \geq 1, \quad (7)$$

where $(\alpha + 1)$ is the ratio of the densities of states (Fe to Au), and $Q_0 [= Q_1(1 + \frac{1}{12}\alpha)]$ is a constant independent of n . Similarly, one may expect the isomer-shift change per iron neighbor (δ_n) to depend on the number of iron neighbors, i. e.,

$$\delta_n = 12 \delta_0 / (12 + \gamma n), \quad (8)$$

where $\delta_0 = \delta_1(1 + \frac{1}{12}\gamma)$ and $(\gamma + 1)$ is the effective ratio of the densities of states (Fe to Au). As a first

approximation one could have $\alpha = \gamma$. An attempt was made to fit the data using this restraint, but the essential feature of the high-concentration spectra, namely, the occurrence of a narrow and a broad line, was not reproduced to the extent observed in the data. Satisfactory fits were obtained putting $\gamma = 0$, i. e., $\delta = \delta_n$ independent of the number of neighbors (n).

This represents the final model. Fits were made allowing all parameters to vary, but due to the large covariances between α and Q_0 , and Δ and δ , some wide variations in the parameters were observed. Taking the general trends, α and δ were fixed (17 and -0.04 mm/sec, respectively), and Δ , Q_0 , and Γ , the linewidth, were allowed to vary. The derived parameters are shown in Fig. 2 as a function of iron concentration, and the fitted curves are shown in Fig. 1 as full lines. The values of χ squared with these restraints were marginally inferior to those obtained allowing α and δ to vary, and in view of the approximations made and possible errors in the atomic concentration of iron, the fits are reasonable. The linewidth has increased from near 0.21 to 0.26 mm/sec to accommodate the broadening due to further neighbors.

2. Temperature Dependence

As noted by other authors,^{5,8} the value of $Q_1 [= 12Q_0/(12 + \alpha)]$ increases with decreasing temperatures, and spectra for the Au-5-at. %-Fe sample obtained at 77, 195, and 298 K have been fitted using the above model, but allowing the relative

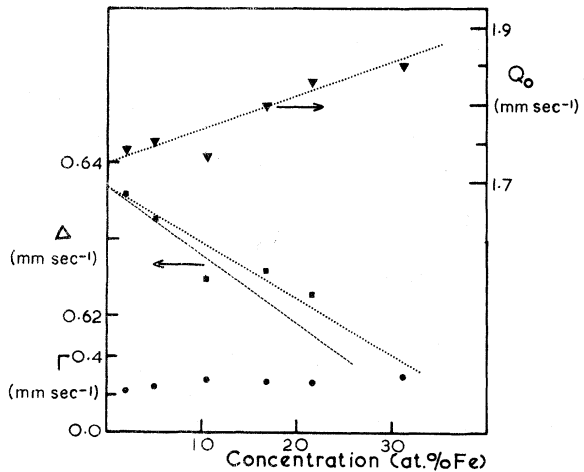


FIG. 2. Parameters derived from the fits in Fig. 1 are shown as a function of iron concentration. The quadrupole interaction at an iron nucleus with one iron neighbor is $12 Q_0/29$ mm/sec, Δ is the isomer shift of the isolated iron atom with respect to α iron (mm/sec), and Γ is the linewidth (FWHM) in mm/sec. The dashed line on the isomer-shift curve is derived from the pressure experiments of Ingalls *et al.* (Ref. 30).

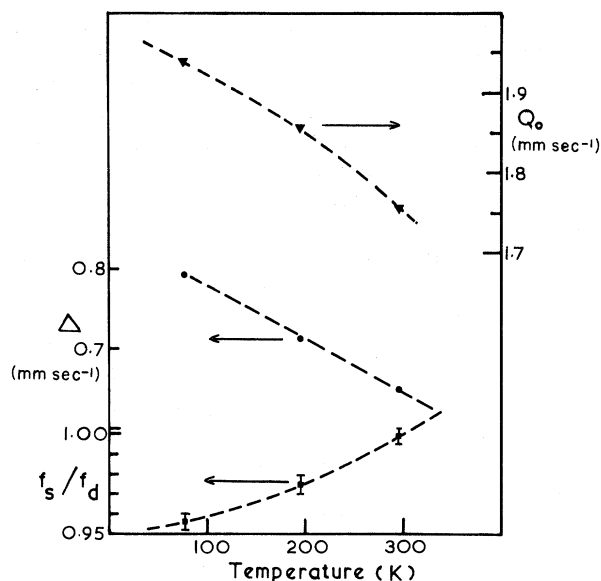


FIG. 3. Results of fitting the spectra of the AuFe 5-at.% sample obtained at 77, 195, and 298 K are shown as a function of temperature. The quadrupole splitting with one neighbor is $12 Q_0/29$ mm/sec, and Δ (mm/sec) is the isomer shift of the isolated iron atom; f_s/f_d is the ratio of the recoilless fraction for isolated iron atoms to that of iron atoms with iron near neighbors.

areas of the contributions from iron atoms with no near-neighbor iron atoms and from iron atoms with one or more iron neighbors to deviate from the ratio set by the probabilities of these configurations in a random 5-at.% alloy. The ratio of the experimental to the calculated relative areas gives the ratio of the mean recoilless fraction for atoms with no iron near neighbors (f_s) to the mean recoilless fraction for atoms with one or more iron neighbors (f_d), provided the iron concentration is known with sufficient accuracy. For the 5-at.% sample, the $n=0$ and $n=1$ configurations are the most probable, and the ratio f_s/f_d gives the ratio of the recoilless fractions of iron atoms with no iron neighbors to that of iron atoms with one iron near neighbor. The results of fitting the spectra at 77, 195, and 298 K are shown in Fig. 3, where Δ , Q_0 , and f_s/f_d are plotted against temperature.

3. Discussion

In the fits described above, the fixing of α and δ effectively defines Q_0 and Δ , respectively, and this should be remembered when assigning any significance to these parameters individually. In Fig. 2, the change in isomer shift of the isolated iron atom as deduced from fitting the data with $\delta = -0.04$ mm/sec is shown. The dashed line in Fig. 2 depicts the change in isomer shift expected from the change in lattice parameter, using the pressure results of Ingalls *et al.*,³⁰ and this line lies very close

to the derived parameters. This good agreement suggests that in these alloys there is very little change in the matrix with the addition of iron, i. e., an isolated iron atom in a 1-at.%-Fe alloy and in a 30-at.%-Fe alloy finds itself in very similar environments. Each iron atom presumably donates one electron to the conduction band, the remaining electrons being accommodated in the virtual d bound state on the iron atom, perhaps spreading on to the near neighbors.

The agreement between the concentration variation of Δ and that expected purely on the basis of the change in lattice parameter supports our choice of the value of γ as zero. A value of $\delta = -0.04$ mm/sec was definitely correct for $n=1$ from the good fit achieved for the 5-at.%-Fe sample, and it seems to remain constant with increasing iron concentration. This is in marked contrast to the behavior of the point charge describing the distortion per neighbor, as it decreases rapidly with increasing numbers of iron neighbors. The quadrupole interaction measures the spatial distribution of all electrons, principally the d electrons in the iron virtual bound state, while the isomer-shift change measures the change in s electron density at the Fe^{57} nucleus.²⁹ The changes in these parameters with numbers of neighbors are therefore not necessarily tied together, and the small change in s electron density is consistent with the much lower s electron density of states compared with the d electron density of states in the virtual bound d state on the iron neighbor. If the ratio of s electron density of states (Fe to Au) is a small number (< 2) then a small dependence of δ on the number of neighbors is expected.

The isomer shift for iron in gold is large for a metallic host (0.637 ± 0.004 mm/sec), and should be compared with the isomer shift in the isoelectronic matrix, copper (0.222 ± 0.004 mm/sec).²⁸ This large increase must be due to the increase in lattice parameter. Using the plot of Walker *et al.*^{29,31} to derive the configuration of electrons, assuming an electrically neutral configuration, i. e., $3d^{8-x}4s^x$, one finds $x=0.9$ for copper and $x=0.7$ for gold. The isomer-shift change induced by one iron neighbor (i. e., -0.04 mm/sec) corresponds for gold to a change of x from 0.7 to 0.72, i. e., by 0.02 of an electron changing from a $3d$ to a $4s$ state. Alternatively, keeping seven $3d$ electrons, the change corresponds to $+0.03$ of a $4s$ electron. Changes in the spatial distribution of the screening electrons with the change of lattice parameter or with the presence of iron neighbors will also change the isomer shift, but the figures given above do illustrate how small the changes need to be.

In the fitting, values of α in the range of 13–20 produced satisfactory fits, and the concentration

dependence of Q_0 shown in Fig. 2 should not be considered unique. It is, however, possible to state that Q_0 does not change much with iron concentration, and the results suggest an increase with concentration. This is to be expected on the Thomas-Fermi-type model, where the contraction of the lattice, besides altering the radial distribution of electrons (and hence Q_0), will tend to force more electrons to concentrate on the iron-iron axis. There could also be changes in other parameters, such as the shape in energy of the virtual bound state.

The magnitude of the quadrupole splitting observed when an iron neighbor is present (0.74 mm/sec) is much smaller than is observed in ferrous compounds. The quadrupole splitting of the Fe^{57} excited state expected for one d electron in a pure orbital state is of the order of 3 mm/sec,^{22,32} and assuming that the antishielding factors and covalency effects in the metal and in the ferrous compounds are similar, an asymmetry of charge given by 0.25 electron in a $3d$ state is indicated. Using the value of α derived from fitting the 300-K data, i. e., 17, the distortion for $n=1, 2, 3, 4$ iron neighbors amounts to 0.25, 0.10, 0.065, and 0.048 of a $3d$ electron per neighbor, respectively. One can see that the necessary asymmetry is small.

The values of α which fit the data (13–20) are considerably larger than the expected ratio of the local densities of states on iron and gold in gold. For iron in gold, the virtual-bound-state model leads to 1.3 per eV for the local density of states for iron in gold,¹⁹ and one obtains 0.27/eV for gold using a free-electron model¹⁶; i. e., the ratio of the densities of states is approximately 4. The assumption of a linear dependence of the distortion on the local density of states is not necessarily correct and was chosen initially for its simplicity. It has been assumed that the point charge produced is proportional to an angular redistribution of the screening charge, but as the electric field gradient depends strongly on the radial distribution both directly (covalency effects) and through the antishielding factor,²⁴ these are also important. In view of all these effects, a power-law dependence of the effective point charge on the ratio of the density of states is not unexpected, and an exponent in the range 1.5–2.5 is indicated by these results. It is also possible that it is the ratio of the densities of d -like states on the iron and gold atoms which determines the value of α , and this ratio will be much larger than 4.

The results may also be explained in terms of the Friedel oscillations of charge^{33,34} around an impurity, regarding neighbors as essentially independent. In this case the factor reducing Q with increasing number of neighbors will be the blurring of the Fermi surface in k space. However, the

results are adequately explained on the model presented above, and the electrostatic interactions which must occur between the two or more iron neighbors have been treated with some degree of consistency.

In Fig. 3, the temperature dependences of the parameters of a 5-at.-%-iron-in-gold sample are shown. The temperature shift for iron in gold has been discussed by other authors^{35,36} and will not be considered here. The temperature dependence of Q_0 is of more interest—it increases by $\sim 10\%$ for a 300-K decrease in temperature,^{6,8} an effect which is not expected on the basis of lattice expansion using the results in Fig. 2. The lattice contraction with decreasing temperature is a small change compared with that on alloying, and the temperature dependence must arise in some other way. If the efg does come from the charge oscillations around impurities, then the sharpening of the Fermi surface with decreasing temperature could increase their amplitude, resulting in an increased quadrupole splitting. Alternatively, due to a similar effect, the shape of the virtual bound state in the conduction band due to the scattering of conduction electrons from the impurity potential could change, leading to an increased density of states at the Fermi energy and a corresponding increase in the efg via the Thomas-Fermi-type model. Also the increasing amplitude of vibration of the iron atom with increasing temperature may cause the iron-screening electrons to redistribute themselves away from the iron axis, resulting in a decrease in the efg at the iron nucleus.

B. Recoiless Fractions

Discussion

The recoilless fractions for iron atoms with iron neighbors and without iron neighbors vary with temperature in different ways. The recoilless fraction f is given by²⁹

$$f = e^{-4\alpha^2 \langle x^2 \rangle / \lambda^2}, \quad (9)$$

where $\langle x^2 \rangle$ is the mean-square amplitude of vibration of the nucleus in the direction of the γ beam and $\lambda = 8.61 \times 10^{-9}$ cm is the wavelength of the radiation. In the Debye approximation this reduces to²⁹

$$T \ll \Theta \quad f = \exp\left[-(R/\Theta)\left(\frac{3}{2} + \pi^2 T^2/\Theta^2\right)\right] \quad (10)$$

and

$$T > \frac{1}{2}\Theta \quad f = \exp(-6RT/\Theta), \quad (11)$$

where Θ is the Debye temperature (an effective Debye temperature for Mössbauer emission), T the actual temperature, and R is the free-atom recoil energy in K ($R = 22.6$ K). The recoilless fraction thus depends on temperature, and also on the direction of emission of the γ ray. The recoilless

fraction at 300 K for isolated iron atoms in gold has been measured, and a value of $f_s = 0.65$ seems appropriate.^{35,37} On a Debye model, one expects the curve of f_s/f_d to start off near 1 at low temperatures, and to deviate away from 1 as the temperature is increased. The behavior shown in Fig. 3 is not consistent with this, and results from an error in the iron concentration used in the fitting. If the iron concentration is decreased from 5.0 to 4.8 at. % iron, the value of f_s/f_d at 77 K will increase to approximately one. The important result is that there is a 5% increase in f_s relative to f_d in going from 77 to 300 K. For such a small increase at 300 K, one can assume that $f_s \approx f_d$ at 77 K giving $f_s = 0.65$ ($\Theta = 310$ K) and $f_d = 0.62$ ($\Theta = 296$ K) at 300 K.

The decrease in the average recoilless fraction f is probably due to a large decrease of f for emission in the Fe-Fe direction, and this large anisotropy will cause some asymmetry in the quadrupole doublet via the Goldanski-Karyagin effect.¹⁵ For a positive electric field gradient, the intensities of the high-energy and low-energy Mössbauer lines are given by²⁹

$$I(\pm \frac{3}{2} \rightarrow \pm \frac{1}{2}) = \frac{3}{2}(1 + \cos^2\theta)f(\theta), \quad (12)$$

$$I(\pm \frac{1}{2} \rightarrow \pm \frac{1}{2}) = (1 + \frac{3}{2} \sin^2\theta)f(\theta),$$

respectively, where the recoilless fraction depends on θ , the angle between the direction of emission and the principal axis of the efg. If there is no change in the Fe-Au spring constants when the iron atom acquires an iron neighbor, the average f ($=0.62$) requires $f=0.45$ along the Fe-Fe axis at 300 K, and the expected asymmetry amounts to 0.95 for the ratio of the intensity of the high-energy line to the intensity of the low-energy line. The anisotropy was not included in the fitting, but it is a general feature of the fits (Fig. 1) that they give more absorption on the left-hand peak and less on the right than is consistent with the data. This symmetry, while small, is significant and supports the Thomas-Fermi model of the screening described earlier; as on this model, a negative electric field gradient is expected. The asymmetry is evident in the spectra of the alloys of high iron concentration despite the proliferation of possible configurations of neighbors. The potential wells describing the efg at the nucleus and the actual atomic motion will be very similar in shape, and the spring constant tensor and efg tensor will have similar principal axes for any particular configuration. The f factor will be related to the spring constant tensor through $\langle x^2 \rangle$, and hence to the efg tensor. On this, simple-model asymmetry is expected in the spectra of Fe^{57} in high-iron-concentration alloys. The decrease in f when the iron atom acquires an iron neighbor is consistent with

results at high temperatures, and can be explained on the basis of the different ionic sizes in these alloys.³⁸

C. Magnetic Interactions

1. Results and Relevant Theory

All alloys were magnetically ordered at 4.2 K,⁵ and the spectra obtained at this temperature are shown in Fig. 4. Because of the large distributions of fields observed at even isolated iron atoms in these alloys (compare the linewidths of the outer and inner lines in the spectrum of the 2-at. % sample), any consistent fitting procedure will involve a large number of parameters to describe the distributions for differing numbers of neighbors. The magnetic moments on the iron atoms are fully polarized at 300 K, and very little change in the iron-electron distribution is expected when the alloys order magnetically. For example, determinations of the hyperfine field at the Fe^{57} nucleus for paramagnetic alloys⁴ (19 T) and magnetically ordered alloys⁵ (22 T) are substantially the same, allowing some polarization due to the magnetic ordering. Hence, the electrostatic interactions measured above the ordering temperatures should be applicable to spectra obtained below the ordering temperatures.

Some general remarks concerning the effects the efg will have on the magnetic spectra are appropriate here. Since the splitting of the excited state

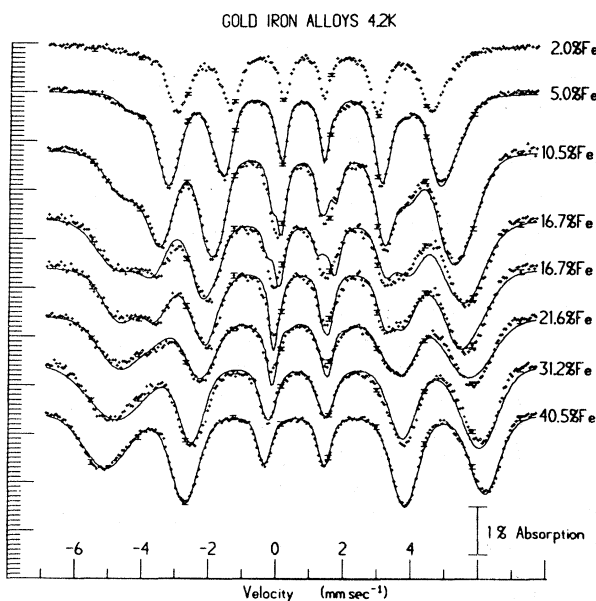


FIG. 4. Mössbauer spectra obtained at 4.2 K together with fitted curves explained in the text are shown. The two spectra for AuFe 16 at. % are to illustrate the alternative fits to the spectrum, and are also explained in the text.

of the Fe^{57} nucleus by the internal magnetic fields of ~ 27 T (~ 2 mm/sec) is substantially larger than that produced by the efg (0.7 mm/sec and reducing for $n > 1$), then one can consider the efg, treated as due to point charges on the near neighbors, as a small perturbation on the magnetic splitting. It is thus sufficient when calculating the effect of the efg due to a configuration of n iron neighbors to find the value of V_{zz} , where z is the magnetic field direction, and treat this as if an axial field gradient with its axis along the z direction; i. e., if a single point charge on an iron neighbor gives a full splitting of $+2q$ above the ordering temperature, then below the ordering temperature, the outer two peaks of the Fe^{57} Mössbauer spectra (labeled 1 and 6) will be shifted by $+\epsilon q$ towards positive velocities, the inner four (labeled 2–5) by $-\epsilon q$, where $\epsilon = \frac{1}{2}(3 \cos^2 \theta - 1)$, and θ is the angle between the magnetization direction and the Fe-Fe direction. For N iron neighbors

$$\epsilon(\beta, N) = \frac{1}{2} \sum_{n=1}^N (3 \cos^2 \theta_n - 1). \quad (13)$$

Because the near-neighbor sites in the face-centered-cubic (fcc) lattice are uniformly spaced over a sphere, then for all possible configurations of N neighbors

$$\sum_{\text{all } \beta} \epsilon(\beta, N) = 0, \quad N = \text{const}; \quad (14)$$

i. e., the centers of gravity of the individual magnetic lines will not shift in energy due to the efg. This is a general property of cubic-random alloys, independent of the easy direction of magnetization. Changes in the easy direction of magnetization cause differences in shape with no shift of the mean position. For example, for the magnetization in a $\langle 100 \rangle$ direction in a fcc lattice, there are two possible values of $\frac{1}{2}(3 \cos^2 \theta - 1)$ for point charges on the 12 near-neighbor sites— $+\frac{1}{4}$ (8) and $-\frac{1}{2}$ (4). For two neighbors, the values of $\epsilon(\beta, 2)$ will be -1 , $-\frac{1}{4}$, and $+\frac{1}{2}$, the amplitudes being distributed so that the mean shift due to the efg is zero.

2. Concentrated Alloys

For most fcc ferromagnets, cobalt, nickel, etc., the easy direction of magnetization lies along a $\langle 111 \rangle$ direction,³⁹ and this direction is probably that assumed by the magnetization in concentrated Au-Fe alloys which exhibit ferromagnetism. The 12 neighbor sites correspond to $\epsilon = \pm \frac{1}{2}$, and no asymmetrical broadening of the lines due to configurations with N neighbors will result. The distribution of $\epsilon(\beta, N)$ is symmetrical with $N+1$ possible values ($N \leq 6$) given by $-\frac{1}{2}N$, $-\frac{1}{2}N+1$, \dots , $+\frac{1}{2}N$. The computed probabilities for the possible configurations with $N=1-6$ are shown in Fig. 5. In the right-hand side of Fig. 5, the abscissa has been corrected to allow for the reducing point

charge derived from the 300-K results.

In the concentrated ferromagnetic alloys, the distributions in Fig. 5 will be relevant, and we can see that despite the proliferation in the possible values of ϵ with increasing N , the electrostatic broadening should decrease. The peaks of the iron resonance for the alloy containing 40 at. % iron are spaced correctly for zero net quadrupole shift, and no asymmetrical broadening of the individual peaks is obvious (Fig. 4). The peak 1 is broader than the right-hand peak 6 for the following reasons. There is a shifting of the spectrum to lower velocities with increasing numbers of neighbors, due to the isomer-shift change (-0.04 mm/sec per iron neighbor), and a shifting of the lines outward from the center due to the increase of magnetic hyperfine fields with iron neighbors. For peak 1 these effects add to give a much broader peak than for peak 6, where the isomer-shift broadening subtracts from the magnetic-field broadening. Because the magnetic shift is proportional to the distance of the peak from the center, peaks 2–5 do not show this effect to such a marked degree.

The full lines in Fig. 4 for the alloys (25–45 at. % Fe) were obtained by fitting six lines with their spacings determined by an internal magnetic field. Each of the six lines consisted of a Gaussian distribution of Lorentzian line shapes of full width half-maximum 0.22 mm/sec. The six widths were unrelated, but the areas were constrained to be in

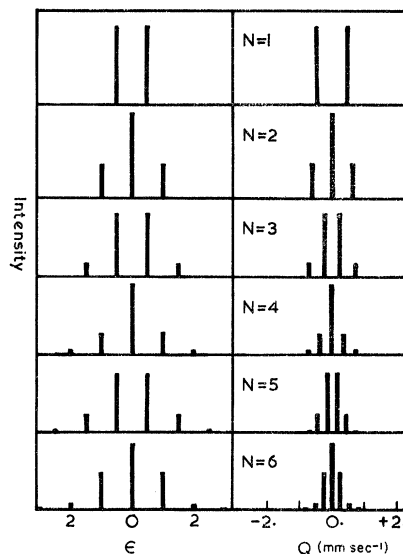


FIG. 5. Distribution of $\epsilon = \frac{1}{2} \sum_{n=1}^N (3 \cos^2 \theta_n - 1)$ expected in a ferromagnetic-random fcc alloy is shown for configurations with $N=1-6$ iron neighbors. The right-hand side (Q) has the abscissa corrected for the reducing point charge used to fit the 300-K results, and converted to actual line distributions in velocity units (mm/sec).

the ratio 3:2:1:1:2:3 for the 31-at.-%-iron sample, i. e., completely randomly magnetized, and in the ratio 3:3.2:1:1:3.2:3 for the 40-at.-%-iron sample, i. e., magnetized in the easy direction closest to the plane of the foil. This magnetization of the foil of the 40-at.-%-iron sample could have resulted from rolling well below the Curie temperature, which is above 500 K. The data for the 40-at.-% sample are fairly well fitted by the model, but the spectrum of the 31-at.-% sample still seems to have some small remaining quadrupole asymmetry, implying that even in this ferromagnetic alloy the magnetization of iron atoms in some regions is not independent of the near-neighbor atomic arrangement (see below).

3. Low-Iron-Concentration Alloys

These samples do not show long-range ferromagnetism,^{3,10,40} and the spin directions when magnetically ordered are presumably determined by the near-neighbor spin arrangement, rather than by a long-ranged effect.^{22,23} In this case, one may expect to see shifts in the spectral components due to electric field gradients (certain spin directions relative to the iron neighbors may be favored), and in Fig. 4, it is evident that such shifts do occur. The broad lines to the left of line 1 for the 5 and 10-at.-%-iron samples do not have a corresponding absorption to the right of line 6.

The restraints on the fitting imposed by the electrostatic parameters derived from the high-temperature data severely limit the possible spin arrangements in these alloys. The fitting was initially based on trial and error, with the Lorentzian linewidth restricted to 0.21 mm/sec full width at half-maximum. In the later stages when the type of model had been decided, a distribution of lines of this linewidth, given by a Gaussian of full width 0.07 mm/sec, was incorporated for each peak account for the electrostatic broadening due to second- and third-nearest neighbors. This was the magnitude of the broadening found in fitting the results in Fig. 1 (see Fig. 2). The following parameters were used in fitting the results in Fig. 4. A mean magnetic field (H) and a half-width (ΔH) of the field distribution around this value, assumed Gaussian in shape, were assigned to configurations labeled by $n=0$ ($H_0, \Delta H_0$), $n=1$ ($H_1, \Delta H_1$), and $n \geq 2$ ($H_2, \Delta H_2$), where n is the number of iron near neighbors to the central atom. The widths of these field distributions arise both from the effects of further neighbors and from the variability in alignment of near-neighbor iron atoms. The relative intensities of the contributions were determined from the alloy concentration C and the relative intensities of the six lines were fixed at 3:2:1:1:2:3, consistent with the magnetization being randomly oriented to the γ -ray beam. The isomer

shift of the isolated iron atom was allowed to vary, the isomer shifts of other configurations being fixed using the 300-K data (-0.04 mm/sec per neighbor). The Gaussian broadening due to the efg from further neighbors was incorporated by adding the 0.07 mm/sec to the full width of the Gaussian describing the magnetic-field broadening, and ultimately folding in one Gaussian of this total width.

No quadrupole interaction would be expected for the isolated iron atom (excluding second-neighbor effects), and no allowance for such an effect was made in the fitting. The configurations with $n \geq 2$, however, do have a resultant efg, and it was necessary to shift the peaks 1 and 6 by -0.24 mm/sec, and 2-5 by $+0.24$ mm/sec about the center of the contribution from these configurations. As discussed earlier, this shows that the magnetization axis is not distributed at random, and it must point in a direction defined by the iron-near-neighbor atomic arrangement. The spin arrangement for $n=1$ is not as well determined by the data, and we have allowed the quadrupole effect, assumed single valued, to vary for these sites.

This represents the final model—six magnetic field parameters, one isomer shift, and one quadrupole splitting were varied to fit the spectra in Fig. 4 for alloys with the 5-, 10.5-, and 16.7-at.-%-Fe alloy (upper spectrum of the two for this alloy). The resulting magnetic-field parameters are shown in Fig. 6, and the quadrupole parameters in Table I.

4. Intermediate-Concentration Alloys

These alloys cover the transition region over which long-range ferromagnetism sets in, i. e., 15-20 at.-% Fe. The fit shown in Fig. 4 for the 16.7-at.-% sample based on the model in (c) (the

TABLE I. Values of electrostatic parameters obtained from fitting the 4.2-K spectra. The quantities marked* were held constant while varying the other parameter.

Iron concentration (at. %)	Number of neighbors	Quadrupole shifting (line 1) mm/sec
5	1	+0.12
	≥ 2	-0.24*
10.5	1	+0.18
	≥ 2	-0.24*
16.7	1	+0.24
	≥ 2	-0.24*
16.7	1	0.18*
	≥ 2	-0.08
21.6	1	0.18*
	≥ 2	-0.05

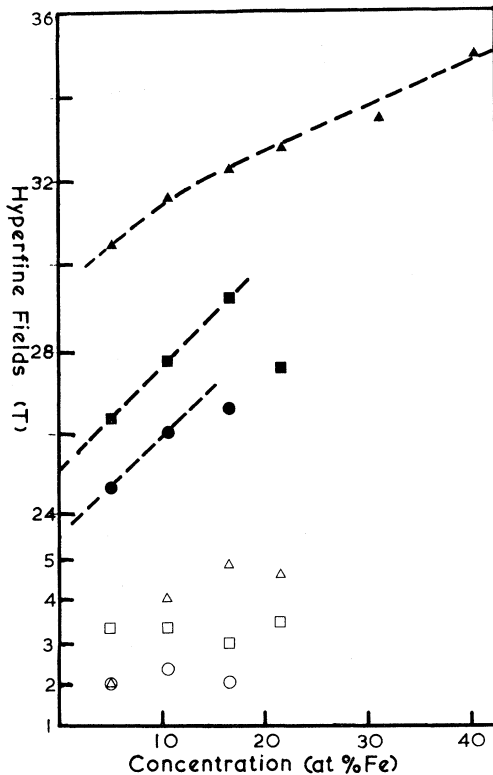


FIG. 6. Hyperfine fields (peak values and the half-width of the distribution) for configurations with $n=0$ (○), $n=1$ (□) and $n \geq 2$ (△) are shown as a function of concentration. The open symbols are the width of the distributions. For the concentrated alloys, the mean fields are shown (▲).

upper curve) deviates from the data in a way which suggests that the shifts of the lines for $n \geq 2$ by -0.24 mm/sec (1 and 6) and $+0.24$ mm/sec (2-5) are too large. We have thus fixed the efg for the configuration having $n=1$ at the value obtained for the 10.5-at. % sample ($+0.18$ mm/sec), and have allowed the averaged value of the efg in the field direction for $n \geq 2$ to vary from ± 0.24 mm/sec. The curve fitted on this model is better for the 16.7-at. % alloy than that obtained keeping this parameter at ± 0.24 mm/sec (Fig. 4, respectively, the lower and upper spectra for the 16.7-at. % sample), and a reasonable fit is also obtained to the spectrum for the 21-at. % sample. The derived parameters are shown in Fig. 6 and Table I.

5. Discussion

Consider the spectra of the more dilute samples (5 and 10.5 at. % Fe), and in particular the configurations described by $n=2$. The point-charge model describing the 300-K data yields a point charge giving ± 0.45 mm/sec quadrupole splitting per neighbor by itself. Hence, if both the point charges were on the magnetic axis, a splitting of ± 0.9

mm/sec in the 4.2-K data is expected. The data give a splitting of -0.48 mm/sec, showing that, since the near neighbors are indistinguishable, $\frac{1}{2}(3 \cos^2 \theta - 1) = \pm \frac{1}{2}$ for each neighbor, i. e., $\theta = \frac{1}{2}\pi$ or $\cos^{-1}(\frac{2}{3})^{1/2}$ for the angle between the Fe-Fe direction and the magnetization axis. The value $\theta = \frac{1}{2}\pi$ seems physically plausible, as the neighbors and the central atom will define a plane, and the spin of the central atom could point normal to the plane. However, the sign of the asymmetry then implies a positive point charge on the iron neighbor, while the Thomas-Fermi-type model and the anisotropy of recoilless fraction indicate a negative point charge. So this is probably the wrong choice of θ .

The other value of θ ($\cos^{-1}(\frac{2}{3})^{1/2}$) defines a $\langle 111 \rangle$ axis with respect to the $\langle 110 \rangle$ direction, and as the high-concentration data are consistent with this direction of magnetization, we suggest that the spin of the iron atoms with two or more iron neighbors lies along one of the now inequivalent $\langle 111 \rangle$ directions. It chooses a $\langle 111 \rangle$ direction so that the number of Fe-Fe axes at an angle of $\frac{1}{2}\pi$ to the magnetization direction is minimized. For configurations of $n=2$ it is possible for $\frac{2}{11}$ of the possible arrangements to choose a $\langle 111 \rangle$ such that $\frac{1}{2}(3 \cos^2 \theta - 1) = \frac{1}{2}$ for both neighbors. The remaining $\frac{9}{11}$ of the arrangements will have all $\langle 111 \rangle$ directions equivalent, with $\frac{1}{2}(3 \cos^2 \theta - 1)$ equal $+\frac{1}{2}$ for one neighbor, and $-\frac{1}{2}$ for the other, leading to zero-resultant-quadrupole effect. The shifts of the lines under these assumptions are consistent with the Thomas-Fermi-type model where the point charge effectively localized on the iron neighbor has a negative sign.

Now consider the situations where the iron atom has one iron neighbor ($n=1$). The obvious symmetry axis is that joining the atoms, but if the localized moment points along this $\langle 110 \rangle$, a large quadrupole asymmetry is expected ($\epsilon = +1$). This is not observed in the spectra and indeed no quadrupole asymmetry of the six narrow lines is evident. Making the assumption that a single value of ϵ is appropriate for $n=1$, the fitting yields $\epsilon = -\frac{1}{3}$ and $-\frac{1}{2}$ for the spectra of the 5- and 10.5-at. %-iron samples, respectively. (These values of ϵ were obtained using the 300-K data and the parameters in Table I.) This suggests that the spin points on a direction closely normal to the Fe-Fe axis, perhaps along a $\langle 111 \rangle$ or $\langle 100 \rangle$ direction normal to the $\langle 110 \rangle$ Fe-Fe axis.

However, the assumption of a single value of ϵ is not as readily justified from the data as in the cases with $n \geq 2$, and a random direction of spin is quite feasible. Fits based on this assumption were almost as good as those based on a single value of ϵ . The model originally suggested by Marshall²² and extended by Klein²³ suggests that something

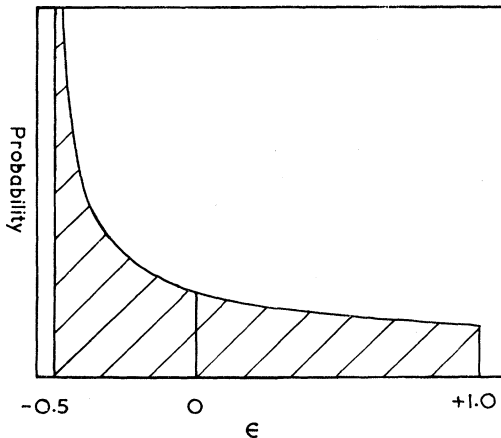


FIG. 7. Distribution of ϵ applicable to the six-line magnetic spectrum due to a small efg oriented at random to the magnetic axis. Peaks 1 and 6 shift by $+\epsilon q$ and peaks 2-5 by $-\epsilon q$, where $2q$ is the splitting produced in the absence of the magnetic field.

along these lines does happen in these alloys, the alignment being controlled by the magnetic interactions due to further neighbors. In this model, one expects a distribution of ϵ similar to that found for the quadrupole interaction due to the broadening introduced by further neighbors; i. e., the probability of ϵ between ϵ and $\epsilon+d\epsilon$ is given by

$$p(\epsilon)d\epsilon = d\epsilon / (\epsilon + \frac{1}{2})^{1/2}, \quad (15)$$

where ϵ goes from $-\frac{1}{2}$ to $+1$. This distribution is shown in Fig. 7 and its principal effect on the spectrum is to broaden the individual lines of the magnetic spectra. So the fitting yields inconclusive results for the spin direction of iron atoms with one neighbor, except that it may be random or at an angle to the $\langle 110 \rangle$ joining the iron atoms such that $\epsilon = -\frac{1}{3}$ to $-\frac{1}{2}$.

In Fig. 6, we have shown the parameters describing the hyperfine-field distributions for the three configurations, i. e., $n=0, 1, 2$. It is interesting to note that two neighbors increase the hyperfine field by three times that for one neighbor. If the field change is due to the redistribution of screening electrons, one expects less than double the increase for one neighbor by analogy with the reducing-point-charge model. However, if the increase comes from a polarization induced by the alignment of near neighbors, one expects deviations from arithmetic additivity as the contributions should be treated as vectors. For $n=2$, one obtains a narrow distribution and a large increase per neighbor, suggesting that all the magnetic moments are aligned parallel. For $n=1$, the wider distribution and small field increase

support the idea that there is more variability in the alignment of the iron atom with only one iron neighbor. However, consistency arguments arise concerning spin directions—a near neighbor to a central atom with $n > 2$ could come in the category described by $n=1$ and hence its spin should not point along the $\langle 111 \rangle$ direction. If the spin of this near neighbor does point along the $\langle 111 \rangle$ direction, the fraction of $n=1$ iron atoms affected is quite small for the 5-at. % Fe sample (~ 0.1), but is significant for the 10.5-at. % Fe sample (0.33). These $n=1$ atoms will have $\epsilon = +\frac{1}{2}$, and the peaks will be shifted by ± 0.19 mm/sec in the magnetic spectra, and will be included with the contributions of the $n \geq 2$ configurations (assuming the parallel arrangement also increases the internal magnetic field significantly). This extra contribution will offset the loss of $n \geq 2$ configurations which have $\sum \epsilon = 0$, as described next. So the fitting is not inconsistent with the arrangement suggested above.

We now consider what happens as the iron concentration is increased. Large clusters of iron atoms ($n > 2$) will become more important, and there will be a preferred spin direction for each cluster, namely, the $\langle 111 \rangle$ axis which maximizes ϵ . However, while some clusters will have large values of ϵ (e. g., $\frac{2}{11}$ of $n=2$ configurations), others will have a small value and a number of different $\langle 111 \rangle$ directions will give this same value (e. g., $\frac{2}{11}$ of $n=2$ configurations have $\epsilon = 0$ for all $\langle 111 \rangle$ directions). Hence there will be a range of values of ϵ from about $\frac{1}{2}n$ to 0, with the mean approaching zero with increasing iron concentration. This is the reason that the quadrupole splitting for $n \geq 2$ configurations decreases in the fitting of the 16.7- and 21.6-at. % iron samples (Table I).

Another effect which occurs with the growth of these clusters with a number of equivalent spin directions is bulk ferromagnetism. On the basis of the theory of Sato *et al.*⁴¹ at about 16 at. % Fe, one will obtain random chains of iron atoms, i. e., clusters with $n \geq 2$, all linked together, and this linked complex will wander through the crystal and in some cases will have almost spherical symmetry. Hence, no $\langle 111 \rangle$ is strongly preferred and applying a field will orient the spins, i. e., bulk ferromagnetism. Also individual clusters with $\epsilon = 0$ will be oriented by the field. The bulk ferromagnetism is not accompanied by any significant changes in the hyperfine fields, and there is little to distinguish between the iron atoms in such clusters in the "antiferromagnetic" and "ferromagnetic" alloys. The transition is a gradual one, and even in the 21.6- and 31.2-at. % iron samples, some quadrupole asymmetry is observed. This shows that in these ferromagnetic alloys there are iron atoms where the local anisotropy is the predominant factor in determining the spin direction, and that ferro-

magnetism does not exist cooperatively everywhere in the alloys.

One parameter which does change abruptly at 16 at. % iron is the slope of the ordering-temperature-vs-concentration curve.³ This is a reflection of the relative strengths of the near-neighbor and next-near-neighbor exchange interactions. The Mössbauer experiments reveal sharp ordering temperatures^{3,5,8} giving a cooperative transition where all moments over all the crystal couple together in a static array. The iron moments within clusters with $n \geq 2$ perhaps align at some angle at temperatures above the bulk ordering temperature, but no information on this point may be derived from the data. These sharp ordering temperatures are a feature of Mössbauer experiments using Fe⁵⁷,^{5,8} Sn¹¹⁹,¹² or Au¹⁹⁷¹⁴ nuclei as probes in this class of dilute alloys (e. g., AuFe, CuMn, RhFe, MoFe) and the ordering temperatures obtained are the same for different isotopes. This and the temperature dependence of the spectra show that these are definite ordering temperatures, and are not associated with relaxation phenomena. Although sharp ordering temperatures were not observed in previous measurements of the susceptibility of Au-Fe alloys,⁴² the recent small-field measurements of Cannella *et al.*⁴³ show that sharp anomalies do exist in the susceptibility at precisely the same temperatures as observed with the Mössbauer effect.

Easy directions of magnetization result from the electronic spins sensing the orbital motion via spin-orbit coupling, and hence preferring certain crystallographic orientations. The problem of spin-orbit coupling in a direct-exchange model was considered originally by Van Vleck,⁴⁴ who showed that the easy directions in ferromagnetic metals could be explained by the pseudodipolar interaction between near neighbors. More recently (see Ref. 45) the theoretical work has been on magnetic compounds. The major term in the solutions is the pseudodipolar interaction, typically an order of magnitude larger than the bare dipole-dipole interaction, and favoring a parallel (or antiparallel) alignment of spins along a certain easy direction. Another term, the anisotropic spin-spin exchange interaction, tends to favor a perpendicular alignment of spins, and will cause the spins to cant from the parallel array.

The screening charge on iron in noble metals is diffuse, and large interactions are expected between near neighbors. The rapid increase in Curie temperature with the formation of linear chains in > 16-at. %-iron alloys shows that the direct-exchange interaction is large, and hence the pseudodipolar interaction and possibly the anisotropic interaction will be sufficiently important to dominate other interactions, such as those due to

further neighbors (indirect exchange via the conduction electrons) or due to applied magnetic fields. Long-range periodicity will not occur. A simpler but physically similar model where only parallel or antiparallel alignments are allowed has been used by Kouvel^{46,47} to calculate the bulk magnetic properties of the related alloy system of manganese dissolved in copper. The results obtained here suggest that such a model may be too simplified, and the inclusion of the preferred magnetization directions in the model may allow a more accurate prediction of the magnetic properties.

IV. CONCLUSIONS

A point-charge model based on a Thomas-Fermi-type of screening has been used to fit the Mössbauer data at 300 K for Au-Fe alloys over a wide concentration range. This model describes the efg as being due to the distortion of the iron-screening charge induced by the high density of states on an iron neighbor, and provides an explanation of the concentration and temperature dependence of the electrostatic parameters. A local model of the alloy appears to hold up to iron concentration as large as 30 at. %. The anisotropy of the recoilless fraction in these alloys also suggests that the sign of the electric field gradient is negative, consistent with an increase in electron density on a line joining the iron atoms.

This negative sign of the electric field gradient is also consistent with a simple model for the magnetic behavior of these alloys. The results can be summarized as follows. For $n = 0$, no information can be derived from the spectra. For $n = 1$, the spin is oriented at random or perhaps at right angles to the Fe-Fe axis. For $n \geq 2$, the spin points along the $\langle 111 \rangle$ direction that makes $\frac{1}{2} \sum_n (3 \cos^2 \theta_n - 1)$ a maximum value [θ_n being the angle between the $\langle 111 \rangle$ and the Fe-Fe(n) axis]. With increasing concentration, one finds an increase in the number of clusters where different $\langle 111 \rangle$ directions may be favored. At 16 at. % Fe, the formation of linear chains of iron atoms becomes very probable, and the clusters interact cooperatively through these chains, the magnetization of each cluster flipping from its own preferred $\langle 111 \rangle$ direction (if different) to the magnetization $\langle 111 \rangle$ characterizing the domain. This is probably not completed throughout the whole crystal until a significantly higher iron concentration. There is no marked increase in the hyperfine fields when this cooperative phenomenon occurs, showing that the iron atoms are fully aligned parallel in their own clusters below this concentration.

The Mössbauer spectra for the high-concentration alloys are characterized by the distributions of quadrupole interactions expected for random ferromagnetic alloys.

ACKNOWLEDGMENTS

The author thanks G. Longworth for his help in some of the experiments and G. Lang, T. Cranshaw, and B. W. Dale for many useful discussions on the behavior of quadrupole splittings when alloys order magnetically. Discussions with M. S. Ridout concerning the results and the use of his curve-plotting program are gratefully acknowledged.

APPENDIX

Consider a point charge α placed on the z axis at unit distance from the origin. The efg tensor ξ is diagonal in the Cartesian system:

$$\xi = \alpha \begin{pmatrix} -\frac{1}{2} & 0 & 0 \\ 0 & -\frac{1}{2} & 0 \\ 0 & 0 & 1 \end{pmatrix},$$

with eigenvalues $V_{xx} = V_{yy} = -\frac{1}{2}\alpha$, $V_{zz} = \alpha$. Now place another charge β in the xz plane at angle θ to the z axis and at unit distance from the origin. The new efg tensor (ξ') in the same axis system is

$$\xi' = \alpha \begin{pmatrix} -\frac{1}{2} & 0 & 0 \\ 0 & -\frac{1}{2} & 0 \\ 0 & 0 & 1 \end{pmatrix} + \frac{1}{2}\beta \begin{pmatrix} 3\sin^2\theta - 1 & 0 & 3\sin\theta\cos\theta \\ 0 & -1 & 0 \\ 3\sin\theta\cos\theta & 0 & 3\cos^2\theta - 1 \end{pmatrix}.$$

First-order perturbation theory gives the new

eigenvalues for $\beta \ll \alpha$:

$$\begin{aligned} V_{zz} &= \alpha + \frac{1}{2}\beta(3\cos^2\theta - 1), \\ V_{xx} &= \frac{1}{2}\alpha - \frac{1}{2}\beta(3\sin^2\theta - 1), \\ V_{yy} &= \frac{1}{2}\alpha - \frac{1}{2}\beta, \end{aligned}$$

i. e.,

$$V_{zz} = \alpha + \frac{1}{2}\beta(3\cos^2\theta - 1)$$

and

$$\eta = |(V_{xx} - V_{yy})/V_{zz}| = 0(\beta/\alpha).$$

The quadrupole splitting observed in the Fe⁵⁷ Mössbauer spectrum S is given by

$$S = A V_{zz}(1 + \eta^2/3)^{1/2},$$

where A includes all constant factors. To order β/α ,

$$S = A V_{zz} = A[\alpha + \frac{1}{2}\beta(3\cos^2\theta - 1)].$$

If β is allowed to move uniformly over a sphere, the probability $P(\theta)$ of an angle θ to $\theta + d\theta$ is given by

$$P(\theta)d\theta \propto \sin\theta d\theta,$$

$$P(S)dS \propto \sin\theta \frac{d\theta}{dS} dS,$$

$$P(S)dS \propto dS/[2\beta(S - \alpha) + \beta^2]^{1/2}.$$

The exact distribution for any value of β could be derived using, for example, the results of Bell.⁴⁸

*Supported in part by the National Science Foundation and the Office of Naval Research.

¹R. J. Borg, R. Booth, and C. E. Violet, Phys. Rev. Letters **11**, 464 (1963).

²P. P. Craig and W. A. Steyert, Phys. Rev. Letters **13**, 802 (1964).

³U. Gonser, R. W. Grant, C. J. Meechan, A. H. Muir, and H. Wiedersich, J. Appl. Phys. **36**, 2124 (1965).

⁴T. A. Kitchens, W. A. Steyert, and R. D. Taylor, Phys. Rev. **138**, A467 (1965).

⁵C. E. Violet and R. J. Borg, Phys. Rev. **149**, 540 (1966).

⁶C. E. Violet and R. J. Borg, Phys. Rev. **162**, 608 (1967).

⁷R. J. Borg, *Atomic and Electronic Structure of Metals* (ASM, Metals Park, Ohio, 1967), p. 41.

⁸M. S. Ridout, J. Phys. C **2**, 1258 (1969).

⁹R. J. Borg, Phys. Rev. B **1**, 349 (1970).

¹⁰C. E. Violet, Develop. Appl. Spectry. **8**, 300 (1970).

¹¹B. Window, J. Phys. Chem. Solids **32**, 1059 (1971).

¹²B. Window, Phys. Letters **24A**, 425 (1967).

¹³A. P. Jain and T. E. Cranshaw, Phys. Letters **25A**, 425 (1967).

¹⁴R. J. Borg and D. N. Pipkorn, J. Appl. Phys. **40**, 1483 (1969).

¹⁵See, for example, V. I. Goldanski and E. F. Makarov, *Chemical Applications of Mössbauer Spectroscopy*, edited

by V. I. Goldanski and R. H. Herber (Academic, New York, 1968).

¹⁶N. F. Mott and H. Jones, *Theory of the Properties of Metals and Alloys* (Oxford U. P., Oxford, England, 1936).

¹⁷J. Friedel, Advan. Phys. **3**, 446 (1954).

¹⁸J. Friedel, Nuovo Cimento Suppl. **7**, 287 (1958).

¹⁹A. Blandin and J. Friedel, J. Phys. (Paris) **20**, 160 (1959).

²⁰E. Daniel, J. Phys. Chem. Solids **23**, 975 (1962).

²¹R. S. Preston, D. J. Lam, M. V. Nevitt, D. O. van Ostenburg, and C. W. Kimball, Phys. Rev. **149**, 440 (1966).

²²W. Marshall, Phys. Rev. **118**, 1519 (1960).

²³M. W. Klein, Phys. Rev. **136**, A1156 (1964).

²⁴G. Lang, Quart. Rev. Biophys. **3**, 1 (1970).

²⁵From the Radiochemical Centre, Amersham, United Kingdom.

²⁶R. S. Preston, S. S. Hanna, and J. Heberle, Phys. Rev. **128**, 2207 (1962).

²⁷See, for example, S. Margulies and J. R. Ehrman, Nucl. Inst. Instr. Methods **12**, 131 (1961).

²⁸B. Window, J. Phys. C **3**, S323 (1970).

²⁹See, for example, G. K. Wertheim, *Mössbauer Effect: Principles and Applications* (Academic, New York, 1964).

³⁰R. Ingalls, H. G. Drickamer, and G. Depasquali, Phys. Rev. **155**, 156 (1967).

- ³¹L. R. Walker, G. K. Wertheim, and V. Jaccarino, *Phys. Rev. Letters* **6**, 98 (1961).
- ³²C. E. Johnson, *Proc. Phys. Soc. (London)* **2**, 748 (1967).
- ³³W. Kohn and S. H. Vosko, *Phys. Rev.* **119**, 912 (1960).
- ³⁴E. Daniel and J. Friedel, *Low Temperature Physics* (Plenum, New York, 1965), p. 933.
- ³⁵W. A. Steyert and R. D. Taylor, *Phys. Rev.* **154**, A716 (1964).
- ³⁶T. A. Kitchens, P. P. Craig, and R. D. Taylor, *Mössbauer Effect Methodology* (Plenum, New York, 1970), p. 123.
- ³⁷J. G. Mullen and R. C. Knauer, in Ref. 36, p. 197.
- ³⁸M. S. Ridout (private communication).
- ³⁹R. M. Bozorth, *Ferromagnetism* (Van Nostrand, New York, 1959).
- ⁴⁰J. Crangle and W. R. Scott, *Phys. Rev. Letters* **12**, 126 (1964).
- ⁴¹H. Sato, A. Arrot, and R. Kikuchi, *J. Phys. Chem. Solids* **10**, 19 (1959).
- ⁴²O. S. Lutes and J. L. Schmit, *Phys. Rev.* **134**, A676 (1964).
- ⁴³V. Cannella, J. A. Mydosh, and J. I. Budnick, *J. Appl. Phys.* **42**, 1689 (1971).
- ⁴⁴J. H. Van Vleck, *Phys. Rev.* **52**, 1178 (1937).
- ⁴⁵J. Kanamori, *Magnetism*, Vol. 1, edited by G. T. Rado and H. Suhl (Academic, New York, 1963), p. 127.
- ⁴⁶J. S. Kouvel, *J. Phys. Chem. Solids* **21**, 57 (1961).
- ⁴⁷J. S. Kouvel, *J. Phys. Chem. Solids* **24**, 795 (1963).
- ⁴⁸R. D. Bell, *J. Phys. Chem. Solids* **29**, 1 (1968).

Phonon Conductivity of CdTe:Fe⁺² and MgO:Fe⁺²

Neelmani and G. S. Verma

Department of Physics, Banaras Hindu University, Varanasi-5, India

(Received 24 November 1971)

A phenomenological form for ω dependence of τ_r^{-1} is proposed which takes into account a term known as the population-difference factor. The thermal-conductivity-vs-temperature curves for CdTe:Fe⁺² and MgO:Fe⁺² are explained satisfactorily except that there are slight deviations at the low-temperature as well as at the high-temperature side.

I. INTRODUCTION

A number of studies of thermal-conductivity measurements, both at high and low temperatures, on semiconductors and insulators doped with impurities that are magnetic in nature (such as Fe, Mn, Co, etc.) have been reported by Slack and co-workers,¹⁻³ de Goer,⁴ Morton and Lewis,⁵ and Challis *et al.*⁶ The general feature of the K -vs- T curves is that there are dips appearing in them, and the over-all conductivity is reduced considerably in comparison to those for the pure sample, with the reduction depending upon the concentration of impurities. A qualitative explanation for this suppression and the dips has been suggested by Slack¹ in terms of resonant scattering of phonons from the magnetic levels of these ions in the crystalline host.

The first quantitative analysis which employs the known energy levels of the excited states of the impurity ion (as deduced from far-infrared spectroscopy) has been given by Morton and Lewis.⁵ The strength of the spin-phonon coupling has been deduced from spin-lattice relaxation-time measurements which identify an Orbach's process (i. e., in MgO:Fe⁺²). The shape of the theoretical curve is more or less of the same form as the experimental one, whereas the thermal conductivity is

heavily reduced at low temperatures. In fact, this reduction is due to the tail of the Lorentzian line-shape function in Eq. (13) of Ref. 5.

Far-infrared optical absorption of CdTe:Fe⁺² gives four peaks⁷ at 18.6, 54.8, 66.7, and 73.2 cm⁻¹ believed to be due to electronic transitions associated with the d -shell levels of Fe⁺² ion impurities in tetrahedral lattice sites of CdTe. This indicates the possibility of four resonant-phonon-scattering processes that may take place from these levels, each having a different spin-phonon coupling.

Taking a level at 18.6 cm⁻¹, we tried to explain the curve R-87, with the corrected expression given by Morton and Lewis⁵ [Eq. (13) of Ref. 5] for the relaxation rate of phonons due to resonant scattering from the magnetic levels as follows:

$$\tau_r^{-1}(x, T) = \alpha(1/T^3)f(x - x_0)F(x_0)(x/x_0^3), \quad (1)$$

where $x = \hbar\omega/k_B T$, ω is the angular frequency of phonons in rad/sec, $x_0 = \hbar\omega_0/k_B T$, $\hbar\omega_0$ is the energy separation of the resonance level from the ground-state level, and α is an adjustable parameter. Further, $f(x - x_0)$ is the Lorentzian line-shape function and $F(x_0)$ is a population-difference factor derived from Maxwell-Boltzmann statistics. However, the theoretical calculations⁸ were so discouraging that even when the simultaneous ef-